View metadata, citation and similar papers at core.ac.uk
brought to you by CORE
provided by UKM Journal Article Repository

Sains Malaysiana 42(12)(2013): 1727–1733

Analysis of Laser Sintered Materials Using Finite Element Method

(Analisis Terhadap Bahan Kerja Sinteran Laser Menggunakan Teknik Unsur Terhingga)

AHMAD SHAHIR BIN JAMALUDIN* & ABDULLAH BIN YASSIN

ABSTRACT

Invention of milling combined laser sintering system (MLSS) is able to reduce the mould manufacturing time and improve the mould accuracy. Thus, more study is needed to increase the understanding for the laser sintered material machining characteristic to gain benefit from the invention of MLSS. This paper clarified the analysis of laser sintered material machinability with the application of Finite Element Method (FEM). Mild steel AISI1055 was applied in developing the Finite Element model in this study due to its popularity in machinability test and adequate level of data availability. 2D orthogonal cutting was employed on edge design tools with updated Lagrangian coupled thermo mechanical plane strain model. Adaptive meshing, tool edge radius and various types of friction models were assigned to obtain efficient simulations and precise cutting results. Cutting force and cutting-edge temperature estimated by Finite Element Method are validated against corresponding experimental values by previous researchers. In the study, cutting force increases when radial depth increases and lowest error acquired when the shear friction factor of 0.8 was applied. Machining simulation for laser sintered materials estimated lower cutting force compared with mild steel AISI1055 due to lower Young modulus. Higher cutting temperature estimated for machining simulation laser sintered material compared with machining simulation mild steel AISI1055 due to its low thermal conductivity.

Keywords: Cutting force prediction; cutting temperature prediction; Finite Element Method (FEM); friction model; 2D orthogonal end milling

ABSTRAK

Reka cipta sistem sinteran laser berpemotong (MLSS) mampu mengurangkan tempoh penghasilan acuan dan meningkatkan kejituan acuan. Oleh kerana itu, kajian yang lebih mendalam adalah perlu bagi mengukuhkan pemahaman terhadap ciri pemesinan bahan kerja sinteran laser untuk mendapatkan manfaat daripada reka cipta MLSS. Kertas ini menjelaskan tentang analisis terhadap kebolehmesinan bahan kerja sinteran laser dengan meramalkan daya, suhu pemotongan dan perbandingan bersama kebolehmesinan keluli lembut AISI1055 menggunakan teknik unsur terhingga (FEM). Keluli lembut AISI1055 diguna pakai dalam pembikinan model unsur terhingga kerana kepopularannya dalam ujian kebolehmesinan dan kuantiti data yang diperoleh agak memuaskan. Model simulasi untuk reka bentuk mata alat pemotong dihasilkan menggunakan model pemotong ortogon 2D dengan aplikasi formulasi Lagrangian terhadap model satah terikan termo mekanikal. Siratan beradaptif, radius mata pemotong dan pelbagai jenis model geseren digunakan untuk memperoleh simulasi yang efisien dan keputusan yang tepat. Nilai daya potongan dan suhu mata pemotong yang diramalkan akan dibandingkan dengan nilai uji kaji daripada kajian terdahulu. Dalam kajian ini, daya mata pemotong menunjukkan pertambahan nilai apabila kedalaman radial mata pemotong meningkat dan nilai ralat terendah diperoleh ketika faktor geseren ricih, m 0.8 digunakan. Simulasi pemesinan bahan kerja sinteran laser meramalkan daya potongan yang rendah apabila dibandingkan dengan keluli lembut AISI1055 disebabkan pemalar Young yang lebih rendah. Suhu pemotong untuk pemesinan bahan kerja sinteran laser diramalkan lebih tinggi berbanding keluli lembut AISI1055 kerana kekonduksian haba yang rendah.

Kata kunci: Jangkaan daya pemotongan; jangkaan suhu pemotongan; model geseran; pemotong ortogon 2D; teknik unsur terhingga (FEM)

INTRODUCTION

Injection moulding is one of the most flexible and prominent operations for mass manufacture of complicated plastic parts with excellent dimensional tolerance. In the conventional mould manufacturing, mould is prepared from the hardened steel using subtractive processes such as high speed machining (HSM) (Dewes & Aspinwall 1997) and electro discharge machining (EDM) (King & Tansy 2003). These processes are time consuming; therefore, the conventional mould manufacturing is not economic. Additionally, in making a precise mould having a deep rib, tool deflection could cause various negative effects such as chatter, wobble and impact. This issue will result in poor dimensional accuracy. Reducing the tool length is one of the ways to control the tool deflection but capability to produce deep rib on the mould reduces.

Hence, conventional mould manufacturing is unsuitable during production of complicated injection mould.

Application of stereolithography (SL) techniques has decreased the time and cost of mould manufacturing. Moreover, deep rib on a mould can be produced. Still, due to its low flexural stresses, life span of the mould produced from SL is short (Rolamada & Dickens 2007). Introducing Selective Laser Sintering (SLS) where the application of a laser beam to irradiate metal powder in making three dimensional shaped parts. This technique could greatly lessen mould manufacturing time and increase its life span. However, resulting part offers limited accuracy and poor surface roughness (Kalpakjian & Schmidt 2000).

These deficiencies were overcome by the invention of milling-combined laser sintering system (MLSS), which integrates laser sintering of fine metallic powder with high speed machining. Ball end mill with a small or micro diameter is employed to machine complex mould features. This is because the ball end mill capable of machining free-form surfaces (Guzzel & Lazuli 2004). Therefore, making deep ribs on complicated mould is achievable and the dimensional accuracy is also enhanced. About 30% of the total production time is required for high speed machining (HSM) in making a mould (Yassin et al. 2009). It is critical to comprehend the machinability of the laser-sintered material, where cutting the laser-sintered material effectively is one of the important factors in gaining utmost economic benefit from MLSS (Yassin 2009). Machinability of workpiece materials refers to the reduced difficulty with which a given metal can be machined to an acceptable surface finish (Kalpakjian & Schmidt 2000). Materials with good machinability require less cutting force, lower processing time, better surface finish and cause small gradual failure on cutting tool. Surprisingly, fewer concerns were given by the researchers for machinability study of laser-sintered material and it can be considered as difficult to machine (Yassin 2009). Since laser sintered material is powder metallurgical base material, its porousness causes satisfactory surface roughness hard to be obtained, although low cutting force is needed to cut the materials (Yassin 2009). Hence, machinability study of laser sintered material is a key factor in gaining the advantage of MLSS as a new invention in mould making.

In this study, machinability of laser-sintered material was analyzed with mean of cutting force and cutting temperature generated on the cutting tool during the machining process by FE simulation. In addition, comparison with the machining processes by FE simulation of mild steel; AISI1055 was also done.

FINITE ELEMENT ANALYSIS (FEA)/FINITE ELEMENT METHOD (FEM)

Finite element analysis (FEA) or also called finite element method (FEM) is a numerical solving technique of dividing a problem into small finite regions called elements. Finite element method (FEM) has been established as one of the method in simulating high speed machining and deem to be beneficial in cost and time saving. Furthermore, FEM has been used to forecast effect of cutting parameter on cutting force, cutting-edge temperature and chip formations (Filice et al. 2008; Ozel 2006). Moreover, cutting forces and temperatures acquired can be used in estimating the ideal cutting conditions such as cutting speed and cutting depth with the implementation of FEM.

One of the most simplified models of FEA for machining is 2D orthogonal cutting. Orthogonal cutting involved cutting edge moves perpendicular to the relative motion between cutting tool and workpiece to remove unwanted material from the workpiece with constant uncut chip thickness (Filice et al. 2008). The earlier researchers developed 2D orthogonal cutting such as Usui and Shirakashi (1982) obtained steady state cutting using the iterative convergence method in FEM. Strenkowski and Carroll (1985) developed numerical model without a preformed chip using updated Lagrangian code. In these models, the effect of uncut chip thickness was neglected since 2D orthogonal cuttings were common in simulating turning processes. In favor of milling operation, uncut chip thickness is inconstant, depends on fix parameters of radial depth, cutting tool diameter and cutting feed and cutting-edge position (Ozel 2006).

The current 2D model developed by Filice et al. (2008) and Özel (2006) applied friction condition in acquiring more useful data. Davim and Maranhao (2009) studied plastic strain and plastic strain rate in machining AISI1045 FEM simulation to observe its effect in cutting process. Updated Lagrangian formulation on 2D thermo mechanical plane strain FEM model will be assigned for the study.

In this study, laser sintered material will be applied as main material properties and AISI1055 will be the comparison. Previously, Furumoto et al. (2010) and Yassin (2009) studied the machinability of laser-sintered materials by doing the comparison with the mild steel AISI1055 machinability experimentally without FEM analysis. Therefore, application of FEM could extend the knowledge of MLSS and laser sintered material.

METHODS

Figure 1 shows the 2D orthogonal finite-element models that were developed based on the ball end mill geometry from the experimental study and also inspired by previous FEM machining models that has been developed by previous researchers (Filice et al. 2006; Ozel 2006; Yassin 2009). The model was developed only for a small part of the tool where the main contact between tool and workpiece occur. Table 1 shows the summarization of the cutting tool characteristic in this study.

In 2D analysis, complex ball part of the end mill was simplified where the maximum effective radius, R_{ef} was considered as the cutting tool rotation radius in acquiring cutting force and cutting temperature prediction. The size of rotation radius relies on the type of ball end milling procedure during the experiment. Figure 2 shows the diagram of the peripheral milling process.

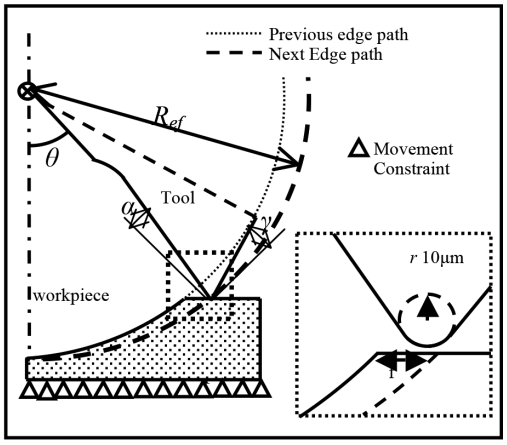

FIGURE 1. Simplified tool and workpiece FEM model

TABLE 1. Cutting tool geometry

Tool diameter, D (mm)	6.0
Tool maximum effective radius of revolution, R_{ef} (mm)	3.0
Tool rake angle, α (°)	5.0
Tool clearance angle, γ (°)	12.0
Tool edge radius, r (mm)	0.01
Feed rate, f (mm/tooth)	0.01

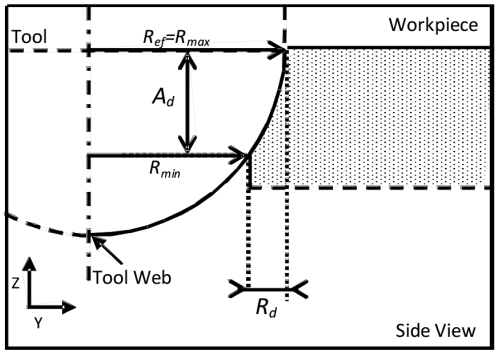

FIGURE 2. Peripheral milling on side view

In this study, the tool geometry was adjusted to the experimental approach of peripheral milling by Yassin et al. (2009). Peripheral milling is the process where teeth located on the periphery of the cutter body generates the milled surface.

Commercially available FE software capable of executing isoparametric quadrilateral meshing and adapted remeshing technique was applied. This type of mesh provides low element requirements and arbitrarily rotatable (Ergatoudis et al. 1968). Adapted remeshing technique was applied where this technique able to remesh the model if critical element distortion existed during the simulation (Filice et al. 2008; Ozel 2006).

Denser and fine meshes were only assigned at the tool edge-workpiece contact area where main mechanical work and large elastic-plastic deformation were generated. This meshing method will ensure lighter and precise simulations can be done in the investigation. Two thousand elements were used for the workpiece and 1000 elements were used for cutting tool mesh. Figure 3 shows an example of isoparametric quadrilaterals mesh with mesh density control that was applied in this study.

Following are the assumptions made to simulate the complex procedure of metal cutting with FEM.

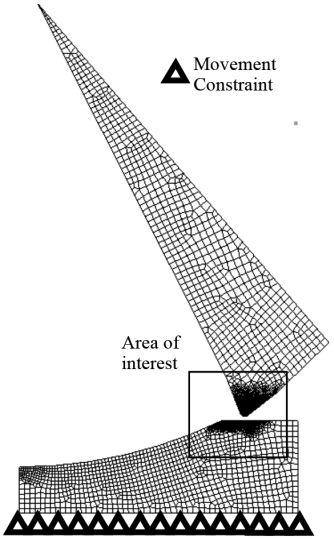

FIGURE 3. Model meshing and density

CONTACT LENGTH

Equation (1) shows contact length model was used as tool-workpiece contact length assumption in the simulation, base Kato et al. (1972), where L_c is tool-workpiece contact length and h in the undeformed chip thickness.

$$L_c = 2h. \tag{1}$$

CONSTANT FRICTION

Constant friction was assumed for all interaction between tool-chip and tool-workpiece. The type of friction model used in this study is called shear friction model. Frictional stress on the rake face of the tool is assumed constant and low stress variation of frictional stress, τ and normal stress, σ_n are neglected (Ozel 2006). This can be expressed by (2).

$$\tau = mk, \tag{2}$$

m is friction factor from 0.6 to 0.9 (will be used in this study) and k is shear flow stress of the work material.

HEAT GENERATION

Heat generation due to metal cutting Q_r (W) is equal to the rate of energy consumption during metal cutting, as shown by (3) and distributed between tool, workpiece and chip.

$$Q_r = W_c = F_v V. \quad (3)$$

F_v (N) is the cutting force and V (m/sec) is the cutting speed. Heat flux, q (W/mm^2) may be acquired from the simulation as (4) (Coelho et al. 2007).

$$q = Q_r / L_c b. \quad (4)$$

L_c (mm) and B (mm) is the contact length and cutting width.

THERMAL BOUNDARIES

Thermal boundary conditions are critical in calculating the temperature distribution in metal cutting simulation. In Figure 4, C'-C" defined the contact between the tool and the workpiece is assumed thermally perfect and a large value of h = 1000 (kW/m^{2}K) is employed (Abukhshim et al. 2005). Heat loss due to convection at the free surface of the tool and the workpiece is defined to be caused by convection. According to Filice et al. (2008), the heat convection coefficient of 20 (W/m^{2}K) is employed for B-C', C"-A, H-D and D-E. The boundary sufficiently far apart from the cutting zone is assumed to be uninfluenced by cutting temperature and thus, boundaries A-B, E-F and F-G are fixed with environmental temperature, 20°C (Abukhshim et al. 2005). Heat loss due to radiation is neglected.

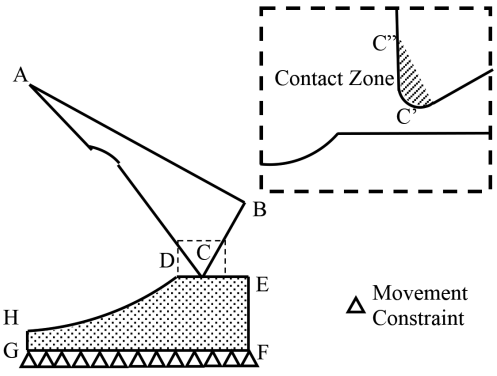

FIGURE 4. Thermal boundaries on tool and workpiece

DATA COLLECTIONS

In validating the estimated cutting edge temperature with the experimental results, air cutting time and cooling effect have to be taken into account. According to Hosokawa et al. (2004), the temperature at a given time after the tool finishes cutting the workpiece is given by (5).

$$T_\psi(\delta) = (T_r - T_0)e^{-a\delta} + T_r. \quad (5)$$

T_ψ (°C) is the temperature at a given air cutting time, T_r (°C) is the instantaneous cutting temperature after tool finishes cutting the workpiece, δ (s) is the air cutting time, T_0 is the room temperature and a = 0.3 is the cooling constant which is determined from Hosokawa et al. (2004). Experimental results by Yassin et al. (2009) measured by optical fiber positioned at 180° from the cutting exit as shown in Figure 5.

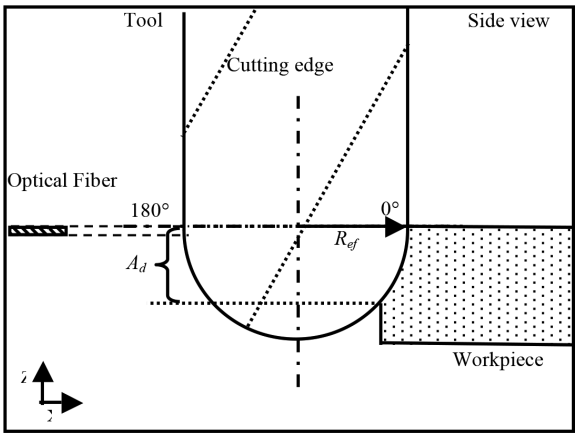

FIGURE 5. Temperature measurement schematic

MATERIALS AND CUTTING CONDITIONS

The laser sintered material properties were taken from the inner surface of work material where metallic powder is assumed fully melted by heating and reheating process, which is 1.0 (mm) from the peripheral surface (Yassin 2009). The value of material hardness increases from 211 ($HV_{0.3}$) to 275 ($HV_{0.3}$) when metallic powder was sintered with low energy density, 2.0 (J/mm^2) to medium energy density, 9.0 (J/mm^2). In addition, the value of material density also shows increasing value from 6950 to 7680 (kgm^{-3}). Nonetheless, nearly identical value of material hardness, 270 ($HV_{0.3}$) and density 7680 (kgm^{-3}) acquired when the metallic powder was sintered with high-energy density, 20 (J/mm^2).

Table 2 shows the properties of metallic powder before it was sintered with medium energy density, 9.0 (J/mm^2) to form laser sintered material, LSMeρ9. Material properties and cutting conditions are shown in Tables 3 and 4 (Yassin et al. 2009).

RESULTS AND DISCUSSION

FEM estimated cutting force and cutting edge temperature in the study are validated against corresponding experimental values by previous researchers (Yassin 2009).

CUTTING FORCES ANALYSIS

Figure 6 shows cutting force profile acquired from the simulation. Cutting force profile shows almost similar values obtained from the simulation due to the rigid tool

TABLE 2. Properties of metallic powder

Materials	SCM	Ni	Cu
Powder density (kg/m^3)	4690	4040	4690
Specific heat (J/kgK)	450	490	380
Thermal conductivity (W/mK)	0.13	0.17	0.17
Particle diameter (μm)	30	30	30
Percent of composition (%)	70	20	10
SCM : Chrome Molybdenum Steel			

TABLE 3. Tool and workpiece material properties

Materials	WC (Tool)	LSMEρ9	AISI1055
Young modulus, E (GPa)	650	124	250
Poisson ratio, ε	0.25	0.3	0.3
Thermal conductivity, k (W/mK)	15	10	53
Density, ρ (kgm^{-3})	14900	7680	7850
Specific heat, c (J/kgK)	334	450	486
Hardness vickers, ($HV_{0.3}$)	1400	275	145

TABLE 4. Cutting conditions

Cutting tool diameter, D (mm)	6.0
Radial depth of cut, R_d (mm)	0.1-0.6
Revolution speed (RPM)	4000-40000
Cutting speed, V_c (m/min)	75-754
Cutting feed, f (mm/tooth)	0.01

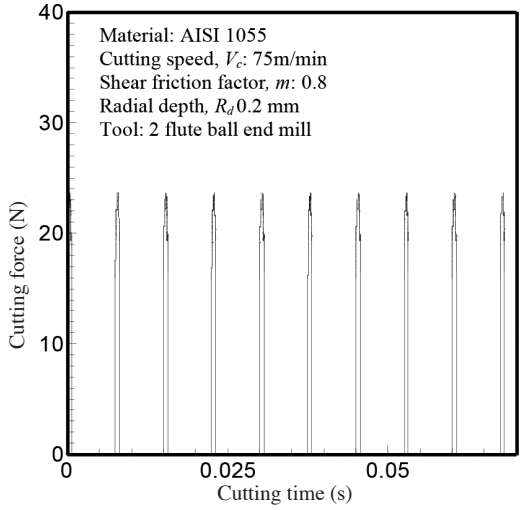

FIGURE 6. Cutting force profile

assumption. In the analysis, a single peak value was taken and the comparison of different shear friction models and radial depths for AISI1055 shown in Figure 7 at cutting speed 75 m/min.

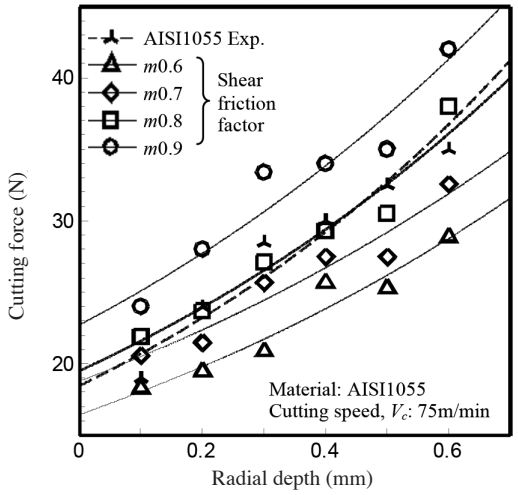

FIGURE 7. Effect of frictions model and radial depth on cutting force

Shear friction factor, m and radial depth, R_d show a direct relation on cutting force according to Figure 7. This is due to increasing frictional stress across the rake face and chip removal rate (mm^3/s). Shear friction factor, m 0.8 can be considered as the best shear friction model in estimating cutting force. This is due to the lowest errors (10%) shown and with this shear friction model, high-precision simulation results that affiliated with cutting force such as cutting temperature could be acquired (Filice et al. 2008).

Identical simulation models were applied on machining process laser sintered material, LSMEρ9with the same shear friction factor, m 0.8. The comparison between simulation and experimental results for AISI1055

and LSMEρ9 are shown in Figure 8. The figure shows that cutting force of AISI1055 is higher than LSMEρ9 at the same cutting rotational speed. This is because LSMEρ9 is easy to deform due to lower Young modulus (124GPa) compared with AISI1055 (250GPa).

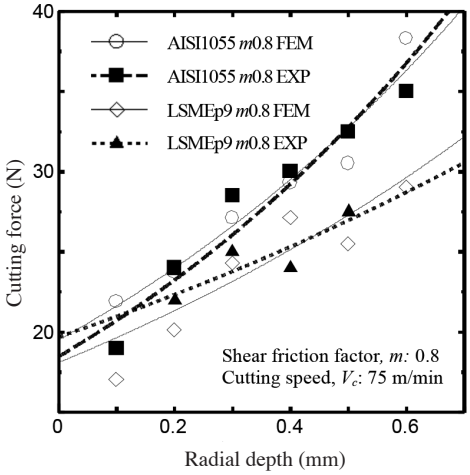

FIGURE 8. Effect of Young modulus and radial depth on cutting force

CUTTING TEMPERATURE ANALYSIS

Figure 9 shows the temperature profile for machining LSMEρ9 at cutting speed 754 m/min and 0.1 mm radial depth at 0° (Figure 5). A single maximum value was taken as the maximum cutting temperature.

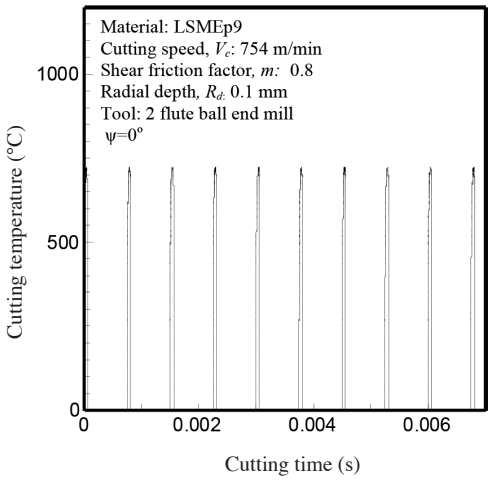

FIGURE 9. Cutting temperature profile

Figure 10 shows the comparisons between estimated cutting temperature of LSMEρ9 and experimental results after considering the cooling effect during the cutting process base on (5). From the figure, error below 5% is shown in FEM simulation of LSMEρ9 when compared with the experimental results. Additionally, the comparison between LSMEρ9 and AISI1055 estimated cutting temperature was also done and LSMEρ9 shows higher cutting temperature than AISI1055.

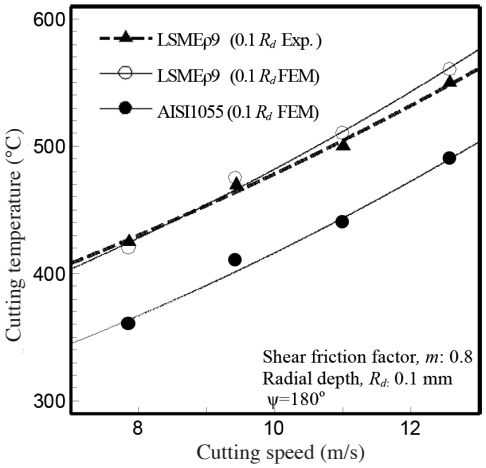

FIGURE 10. Effect of cutting speed on cutting temperature

Figure 11 shows the steady state analyses for temperature distributions inside the workpiece when machining both materials at 754 m/min was done. The workpiece temperature at the tool tip for LSMEρ9 is higher than AISI1055. However, cutting temperature decreases significantly for LSMEρ9 workpiece along the cross sectional compared with AISI1055 workpiece. This is due to the amount of heat travels inside LSMEρ9 workpiece is lower than AISI1055 in single unit time, where LSMEρ9 has lower thermal conductivity (10 W/mK) than AISI1055 (53 W/mK). Heat becomes harder to conduct away from heat source for material with low thermal conductivity (Kalpakjian & Schmidt 2000; Yassin 2009).

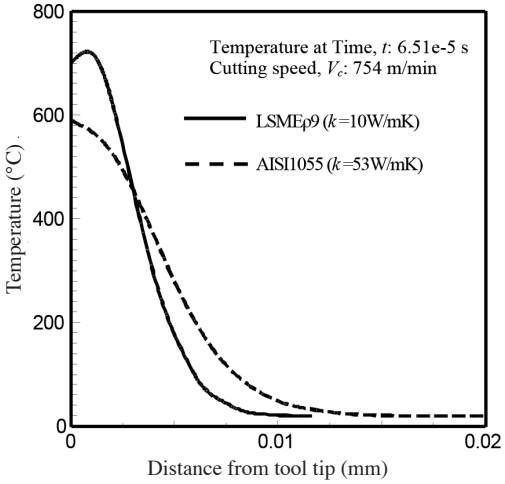

FIGURE 11. Temperature distribution comparison for different thermal conductivity

CONCLUSION

In this study, machinability of laser sintered material (LSMEρ9) was analyzed by estimating cutting force and cutting temperature using FEM and compare with mild steel AISI1055 analysis results. 2D orthogonal cutting with thermo-mechanical plane strain model were applied.

Constant shear friction factors, *m* range between 0.6-0.9 is used in the study and validated with the experimental results. Lowest error (10%) shown for estimating cutting force using a shear friction factor, *m* 0.8. The cutting force increases with the increase in shear friction factor and radial depth of cut, R_d due to increasing frictional stress and chip removal rates (mm^3/s). Cutting speed shows direct influence to cutting edge temperature due to increased cutting energy. Lowest errors (5%) shown for estimated cutting temperature on AISI1055 and LSMEρ9 when validated with experimental results. AISI 1055 shows higher cutting force but lower cutting edge temperature than laser-sintered materials, LSMEρ9 due its higher Young modulus and lower thermal conductivity.

From the study, laser sintered material, LSMEρ9 can be considered having low machinability compared with mild steel due to higher cutting temperature.

ACKNOWLEDGEMENTS

The authors would like to thank the Ministry of Higher Education Malaysia (KPT) and Universiti Malaysia Pahang (UMP) for funding the master study.

REFERENCES

Abukhshim, N.A., Mativenga, P.T. & Sheikh, M.A. 2005. Investigation of heat partition in high speed turning of high strength alloy steel. *Int. Journal of Machine Tools & Manufacture* 45: 1687-1695.

Coelho, R.T., Ng, E.G. & Elbestawi, M.A. 2007. Tool wear when turning hardened AISI 4340 with coated PCBN tools using finishing cutting conditions. *Int. Journal of Machine Tools and Manufacture* 47: 263-272.

Davim, J.P. & Maranhao, C. 2009. A study of plastic strain and plastic strain rate in machining of steel AISI 1045 using FEM analysis. *Materials and Design* 30: 160-165.

Dewes, R.C. & Aspinwall, D.K. 1997. A review of ultra high speed milling of hardened steels. *Journal of Materials Processing Technology* 69: 1-17.

Ergatoudis, I., Irons, B.M. & Zienkiewicz, O.C. 1968. Curved, isoparametric, quadrilateral elements for finite element analysis. *International Journal of Solids and Structures* 4(1): 31-42.

Filice, L., Micari, F., Rizzuti, S. & Umbrello, D. 2008. Dependence of machining simulation effectiveness on material and friction modeling. *Machining Science and Technology* 12(3): 370-389.

Furumoto, T., Ueda, T., Abdul Aziz, M.S., Hosokawa, A. & Tanaka, R. 2010. Study on reduction of residual stress induced during rapid tooling process – influence of heating conditions on residual stress. *Key Engineering Materials* 447: 785-789.

Guzzle, B.U. & Lazuli, I. 2004. An enhanced force model for sculptured surface machining. *Machining Science and Technology* 8: 431-448.

Hosokawa, A., Zhou, Z.P., Yamada, K. & Ueda, T. 2004. Studies on high-speed milling with small ball end mill: Temperature distribution on flank face of cutting tool. *Journal of Japanese Society Precision Engineering* 70: 1527-1532.

Kalpakjian, S. & Schmidt, S.R. 2000. *Manufacturing Engineering and Technology*. 4th ed. New Jersey: Prentice Hall International. p. 1148.

Kato, S., Yamaguchi, K. & Yamada, M. 1972. Stress distribution at the interface between tool and chip in machining. *Trans. ASME J. Eng. Ind.* 94: 683-689.

King, D. & Tansy, T. 2003. Rapid tooling: Selective laser sintering injection tooling. *Journal of Materials Processing Technology* 132: 42-48.

Ozel, T. 2006. The influence of friction models on finite element simulations of machining. *Int. Journal of Tools and Manufacturing* 46: 518-530.

Rolamada, S. & Dickens, P. 2007. Rapid tooling analysis of Stereolithography injection mould tooling. *International Journal of Machine Tools and Manufacture* 47: 740-747.

Strenkowski, J.S. & Carroll, J.T. 1985. A finite element model of orthogonal metal cutting. *Trans. ASME J. Eng. Ind.* 107: 349-354.

Usui, E. & Shirakashi, 1982. Mechanics of machining from descriptive to predictive theory. *On the Art of Cutting Metals-75 Years Later* 7: 13-55.

Yassin, A. 2009. Experimental study on machinability of laser-sintered material in ball end milling. PhD Thesis. Kanazawa University (unpublished).

Yassin, A., Ueda, T., Furumoto, T., Hosokawa, A., Tanaka, R. & Abe, S. 2009. Experimental investigation on cutting mechanism of laser sintered material using small ball end mill. *Journal of Materials Processing Technology* 209: 5680-5689.

Department of Mechanical and Manufacturing Engineering
Faculty of Engineering
Universiti Malaysia Sarawak
94300 Kota Samarahan, Sarawak
Malaysia

*Corresponding author; e-mail: aero_zephyr@yahoo.com

Received: 19 March 2012
Accepted: 30 May 2012